Photochemistry and Photobiology, 2014, 90: 439–447

Interaction of $H_2@C_{60}$ and Nitroxide through Conformationally Constrained Peptide Bridges‡

Luca Garbuio[1], Yongjun Li[2], Sabrina Antonello[1], José A. Gascón[3], Ronald G. Lawler[4], Xuegong Lei[2], Yasujiro Murata[5], Nicholas J. Turro[†2] and Flavio Maran[*1]

[1]Department of Chemistry, University of Padova, Padova, Italy
[2]Department of Chemistry, Columbia University, New York, NY
[3]Department of Chemistry, University of Connecticut, Storrs, CT
[4]Department of Chemistry, Brown University, Providence, RI
[5]Institute for Chemical Research, Kyoto University, Kyoto, Japan

Received 31 August 2013, accepted 11 October 2013, DOI: 10.1111/php.12191

ABSTRACT

We synthesized two molecular systems, in which an endofullerene C_{60}, incarcerating one hydrogen molecule ($H_2@C_{60}$) and a nitroxide radical are connected by a folded 3_{10}-helical peptide. The difference between the two molecules is the direction of the peptide orientation. The nuclear spin relaxation rates and the *para* → *ortho* conversion rate of the incarcerated hydrogen molecule were determined by ^{1}H NMR spectroscopy. The experimental results were analyzed using DFT-optimized molecular models. The relaxation rates and the conversion rates of the two peptides fall in the expected distance range. One of the two peptides is particularly rigid and thus ideal to keep the $H_2@C_{60}$/nitroxide separation, *r*, as large and controlled as possible, which results in particularly low relaxation and conversion rates. Despite the very similar optimized distance, however, the rates measured with the other peptide are considerably higher and thus are compatible with a shorter effective distance. The results strengthen the outcome of previous investigations that while the *para* → *ortho* conversion rates satisfactorily obey the Wigner's theory, the nuclear spin relaxation rates are in excellent agreement with the Solomon–Bloembergen equation predicting a $1/r^6$ dependence.

INTRODUCTION

Endohedral fullerenes are systems in which an atom or a small molecule is incarcerated in the nanocavity of C_{60} and other fullerenes (1–3). A question of central importance in the study and potential applications of these fascinating chemical species is the degree to which the caged molecule "senses" the outside world. An early indication of the subtlety of such communication was the unusual isotope effect on excited state quenching via the hydrogen isotopologues of $H_2@C_{60}$ (4). More recently, the relative isolation of the *endo* hydrogen molecule in $H_2@C_{70}$ has made it possible to prepare and store H_2 molecules enriched in the *para* nuclear spin isomer by photoexcitation of the endofullerene at low temperature (5). The ready availability of such sources of enriched samples of *para*-H_2 is of potential importance to some areas of technology, including magnetic resonance imaging (6).

In the case of $H_2@C_{70}$, the enrichment occurs via paramagnetic catalysis of *ortho–para* conversion by the excited triplet state of the cage. Another photochemical strategy, however, would be to initiate catalysis via photoexcitation of an auxiliary molecule attached to the fullerene cage via a suitable linker. The necessary paramagnetic state could then arise either from a localized triplet excited state of the auxiliary or via photoinduced intramolecular electron transfer between the auxiliary and the fullerene cage to form a linked radical anion–cation pair with unpaired electrons on both the cage and the auxiliary. The former effect would require a remote, localized triplet state. The latter could lead to magnetic catalysis via paramagnets at both the cage and remote sites. A promising recent study has, for example, shown that a radical ion pair can be efficiently formed via a photoexcited singlet state of the endofullerene conjugate $La_2@C_{80}$-exTTF that contains two *endo* lanthanum atoms and a π-extended tetrathiafulvalene (ex-TTF) auxiliary (7). The details of the interaction of *endo*-H_2 with a paramagnetic cage have also been studied for both the C_{60} triplet (8) and a fulleropyrrolidine radical anion (9).

In probing the effectiveness of a remote paramagnet, it has proven useful to employ $H_2@C_{60}$ derivatives covalently linked to a nitroxide radical, in which the distance between the two moieties may be controlled with suitable molecular bridges. In a previous study (10), we synthesized a series of $H_2@C_{60}$ nitroxide derivatives in which the distance (*r*) between the centers of the nitroxide radical and the *endo*-H_2 was varied (Scheme 1). In this case, the nitroxide auxiliary serves as a proxy for a photoderived paramagnetic at the same distance. The longitudinal nuclear spin relaxation rate ($1/T_1$, which is the reciprocal of the nuclear spin relaxation time T_1) of the *endo*-H_2 was found to decrease with an increase in the distance. Quantitative fitting using the Solomon–Bloembergen equation (11,12), which relates the distance of the couple radical/H_2 to the relaxation rate of hydrogen, indicated that the relaxation rate (or inner-sphere relaxivity) is inversely proportional to r^6. However, we note that the spacers that separated the nitroxide radical and the *endo*-H_2 were relatively flexible, which is a parameter making the precise measurement of the actual distance as difficult.

*Corresponding author e-mail: flavio.maran@unipd.it (Flavio Maran)
†Deceased November 24, 2012.
‡This paper is part of the Special Issue honoring the memory of Nicholas J. Turro.

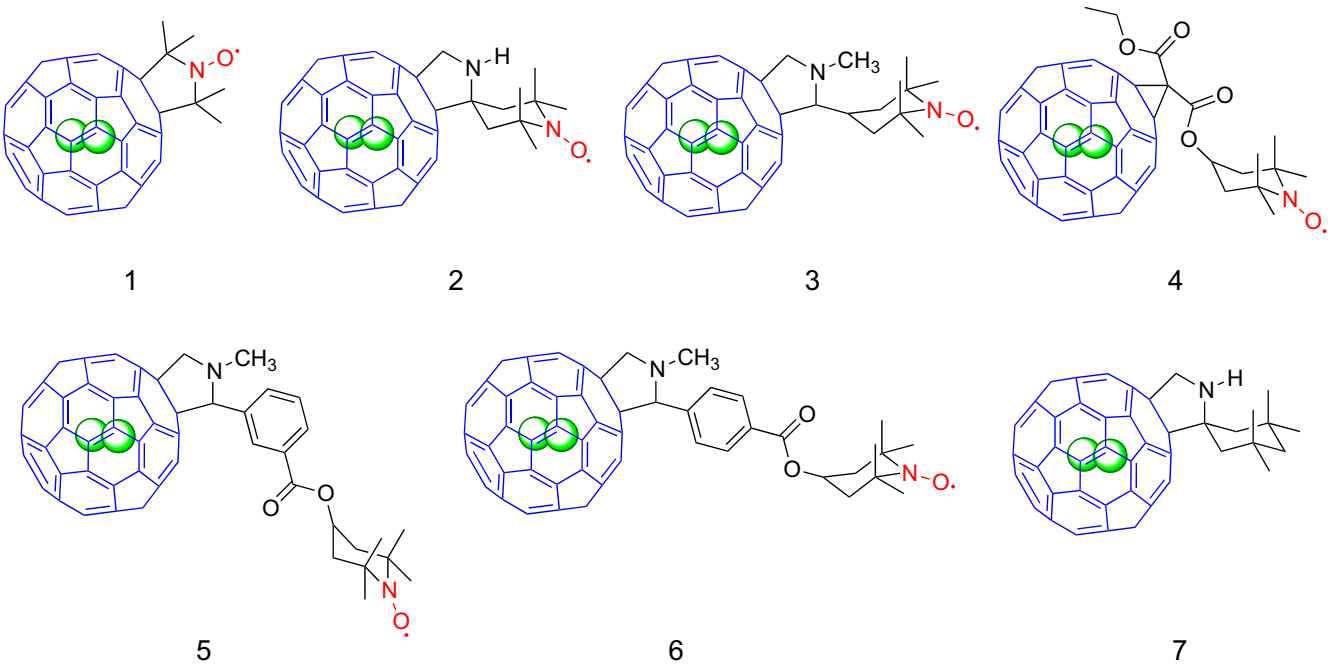

Scheme 1. Chemical structures of $H_2@C_{60}$-nitroxide derivatives previously investigated (10,13). The spheres inside the C_{60} cages represent incarcerated H_2 or HD. Compound 7, in which there is no nitroxide, is a diamagnetic reference.

As noted above, an additional probe of the interaction of *endo*-H_2 is the conversion *para* to *ortho* hydrogen. According to the Pauli exclusion principle, the hydrogen molecule exists as two spin isomers, named *ortho*-H_2, with two spins parallel to each other, and *para*-H_2, with opposite spins. Whereas *ortho*-H_2 is NMR active, *para*-H_2 is NMR inactive. At room temperature, the dihydrogen consists of 75% *ortho*-H_2 and 25% of *para*-H_2, but when the temperature is lowered to 77 K (liquid nitrogen temperature) in the presence of oxygen as a spin catalyst, a 50%:50% composition is attained. The series of $H_2@C_{60}$ nitroxide derivatives of Scheme 1 was employed to assess the distance dependence of the *para*-H_2 to *ortho*-H_2 conversion (13). After obtaining the ~50% composition ratio at low temperature, the conversion of *para*-H_2 to *ortho*-H_2 was monitored at room temperature, with the nitroxide radical moiety acting as the spin catalyst. The conversion rate constant ($k_{p\text{-}o}$) was found to be inversely proportional to roughly the eighth power of the distance *r*: the conversion rates are thus in good agreement with the Wigner's theory (14,15), modified for the intramolecular interaction of H_2 with the paramagnet.

In the present study, we investigated two compounds, in which the nature of the connecting bridge was such that the relative position of the nitroxide radical and the *endo*-H_2 could be efficiently controlled. The bridge was a peptide based on the strongly helicogenic α-aminoisobutyric acid (Aib) residue. Aib-based peptides form 3_{10}-helices and are remarkably rigid even when they are short (16,17), and this property qualifies them as convenient scaffolds for measurements requiring precise control of distance (18). 3_{10}-Helices are characterized by strong intramolecular C = O···H–N hydrogen bonds that make the peptide associated with a strong oriented molecular dipole moment (19,20). These combined properties were previously found to affect significantly, e.g. photoinduced intramolecular electron transfer (21,22) and the redox potentials of gold nanoclusters (20) and electroactive groups (23,24). Very recently, we took advantage of the peculiar properties of Aib peptides in a study focusing on fullerene–peptide–nitroxide systems (Scheme 2, compounds 8+ and 8−) (25). We found that reversing the dipole moment of the peptide helix significantly affects the redox properties of both the C_{60} and nitroxide groups. IR absorption spectroscopy and ^{1}H NMR spectroscopy results also highlighted a strong effect of peptide orientation on the spectral patterns. Time-resolved EPR showed that the C_{60} triplet state of both peptides interacts with the nitroxide radical to form a doublet spin state. However, although the relative distance of the two moieties appears to be very similar, whereas for 8+ the triplet–doublet system is weakly coupled, in 8− the coupling is strong. We ascribed this difference to different orientations of the pairs but also to a different effective distance, which appears to be shorter in the strongly coupled 8− system. Because of the ability of the peptide-bridge orientation to tune physicochemical properties, the main conclusion of the earlier study was that these fullerene–peptide–radical systems cannot be considered as simple C_{60}/nitroxide radical dyads.

This study extends the knowledge acquired on these complex systems to the corresponding analogues containing an *endo*-H_2 molecule. The main target of this study is to assess the dependence of the relaxation and conversion rates on peptide orientation to shed light onto the intriguing results previously obtained (25) on the peptide-orientation dependence of the interaction between C_{60} triplet and nitroxide by separating the effects of distance and electric dipole moment orientation. The use of the incarcerated hydrogen probe strategy is thus meant to provide a necessary piece of information toward this goal: assessing the effective relative distance of the nitroxide with respect to C_{60}. The relaxation and conversion rates are magnetic in origin and should be insensitive to the orientation of the electric dipole moment of the linker. Thus, by following the same synthetic strategies previously adopted for the nonendofullerene systems (25), we synthesized the two $H_2@C_{60}$–peptide–nitroxide systems

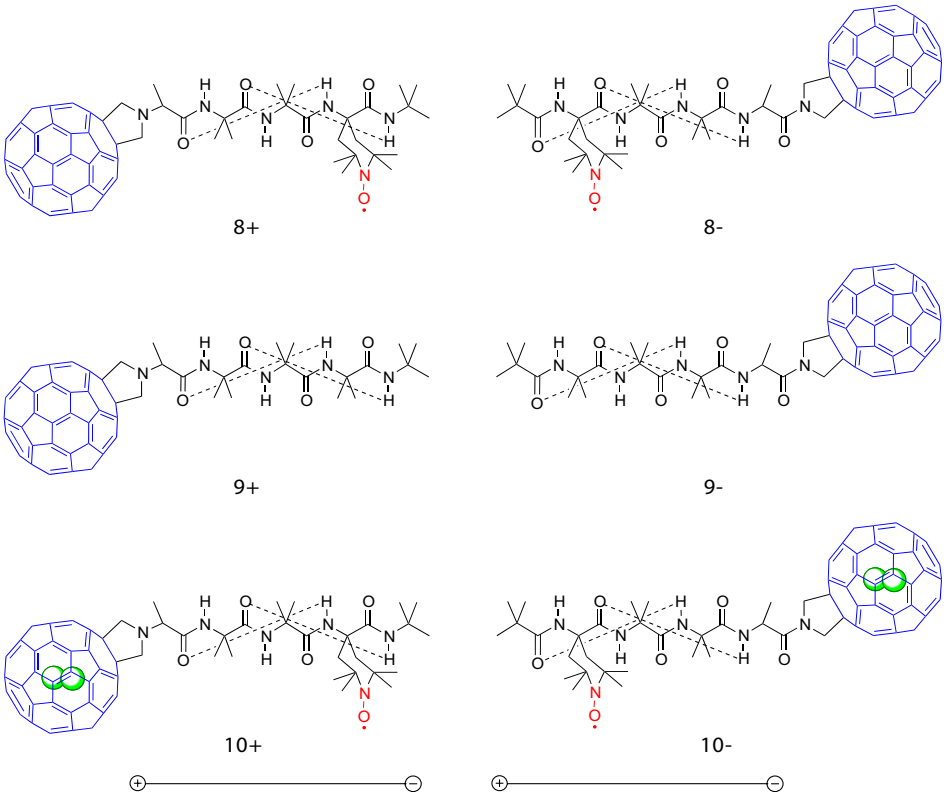

Scheme 2. Structures of 10+ and 10− (the spheres inside the C_{60} cages represent incarcerated H_2 or HD), the nonendohedral fullerene equivalents 8+ and 8− and reference systems 9+ and 9−, where Aib replaces TOAC. The intramolecular H bonds are indicated. The arrows show the direction of the peptide dipole moment.

of Scheme 2. The bridge is a folded helical oligopeptide possessing two intramolecular C=O···H–N hydrogen bonds, and the two compounds differ due to the opposite orientation of the peptide-helix dipole moment. We label the two compounds as 10+ and 10−, where the "+" or "−" sign indicates whether the positive or negative side of the dipole points toward or away the $H_2@C_{60}$ moiety. For the nitroxide, we used the TOAC (2,2,6,6-tetramethylpiperidine-1-oxyl-4-amino-4-carboxylic acid) residue, a tetrasubstituted α-amino acid equivalent to Aib (26). Scheme 2 also shows the nonendofullerene equivalents of 10+ and 10−, *i.e.* 8+ and 8−, and the corresponding reference systems 9+ and 9− in which TOAC is substituted by Aib. The objectives of our study were: 1) to measure the *endo*-H_2 nuclear spin relaxation rates $1/T_1$ (more specifically, $1/T_{1,p}$, where $T_{1,p}$ is the relaxation time solely due to the paramagnetic species) and the *para*-H_2 to *ortho*-H_2 conversion rate constants $k_{p\text{-}o}$ of the two $H_2@C_{60}$-peptide-nitroxide derivatives; 2) to investigate if and how the orientation of the peptide affects $1/T_{1,p}$ and/or $k_{p\text{-}o}$; 3) to verify if the results obtained with the peptide systems 10+ and 10− are consistent with those previously obtained with the compounds of Scheme 1 (10,13). Density functional theory (DFT) calculations provided molecular models used to extract the distance between the $H_2@C_{60}$ core and the nitroxide, as well as simulations of the ^{1}H NMR chemical shifts of the four amide protons of reference compounds 9+ and 9−. Despite the very similar optimized distance, we found that both the relaxation and the conversion rates of 10− are faster than those measured for 10+, which is attributed to quite significant difference in rigidity of the two systems. This outcome is thus in line with other measurements carried out on the nonendohedral equivalents of the investigated peptides (25), and furnishes a key to understand the noticeable difference in time-resolved EPR behavior of 8+ and 8−. Overall, the results strengthen the outcome of previous investigations (10,13), particularly concerning the excellent agreement of the nuclear spin relaxation rates with the Solomon–Bloembergen equation.

MATERIALS AND METHODS

Chemicals. Unless stated otherwise, all commercially available chemicals were used as received. The optically active α-amino acid is of L-chirality. $H_2@C_{60}$ was synthesized as already described (1). Empty fullerene C_{60} (99%), acetonitrile (CH_3CN) (99.5%), Boc-L-Ala-OH (99%; Boc = *tert*-butyloxycarbonyl), *N*,*N*-diisopropylethylamine (99%; DIEA), diethyl ether (99.5%), *N*-ethyl-*N*′(3-dimethylaminopropyl)carbodiimide hydrochloride (99%; EDC·HCl), ethyl acetate (99.5%), paraformaldehyde (95%), trifluoroacetic acid (99%; TFA), toluene (99.5%) were purchased from Aldrich. Ethanol (99.5%) and trifluoromethansulphonic acid (CF_3SO_3H) (98%) were purchased from VWR. 7-Aza-1-hydroxybenzotriazole (HOAt) was purchased from GL Biochem. Choloroform (99.8%) was purchased from Fisher. $(Boc\text{-}Ala)_2O$, 3-trityl-5-oxazolidinone, H-$(Aib)_2$-TOAC-NH*t*Bu, HO(CO)CH_2NHCHCH_3COO*t*Bu, Piv-TOAC-$(Aib)_2$-OH (Piv = pivaloyl or *tert*-butylcarbonyl), Fp-Ala-$(Aib)_2$-TOAC-NH*t*Bu (8+), Piv-TOAC-$(Aib)_2$-Ala-Fp (8−), Fp-Ala-$(Aib)_3$-NH*t*Bu (9+) and Piv-$(Aib)_3$-Ala-Fp (9−) were available from a previous study (25).

*(H_2@Fp)-Ala-Ot*Bu. To a solution of 40 mg (0.055 mmol, 1 equiv) of $H_2@C_{60}$ in 50 mL of toluene, 14.4 mg of HO(CO)CH_2NHCHCH_3COO*t*Bu (0.071 mmol, 1.3 equiv) and 8.1 mg of paraformaldehyde (0.27 mmol, 5 equiv) were added. After 4 h of reflux, the mixture was purified by flash chromatography (3:1 toluene/petroleum ether). A quantity of 10 mg (25% w/w) of unreacted $H_2@C_{60}$ was recovered. Crystallization from toluene/acetonitrile afforded 17.2 mg (yield 35%) of H_2@Fp-Ala-O*t*Bu (Fp = 3,4-fulleropyrrolidine) as a brown solid. R_f (toluene) = 0.6; R_f (7:3 toluene/petroleum ether) = 0.3. ^{1}H

NMR ($CDCl_3$) δ −4.45 (s, *ortho*-H_2), −4.49 (t, J = 41 Hz, HD), 1.64 (s, 9H, *t*Bu), 1.76 (d, J = 7 Hz, 3H, Ala CH_3), 3.93 (q, J = 7 Hz, 1H, Ala CH), 4.62 (s, 4H, Fp $2CH_2$).

*(H_2@Fp)-Ala-(Aib)$_2$-TOAC-NH*t*Bu* (10+). (H_2@Fp)-Ala-OH, obtained from deprotection of (H_2@Fp)-Ala-O*t*Bu (17 mg, 0.020 mmol, 1 equiv) in $CHCl_3$/TFA 50% v/v was added to a solution of 3.4 mg (0.026 mmol, 1.3 equiv) of HOAt and 4.7 mg (0.026 mmol, 1.3 equiv) of EDC•HCl in 15 mL of anhydrous $CHCl_3$ at 0°C, and the resulting mixture was stirred for 1 h at r.t. H-(Aib)$_2$-TOAC-NH*t*Bu (0.024 mmol, 1.2 equiv) was then added to the reaction mixture together with 4.1 μL (0.026 mmol, 1.3 equiv) of DIEA. After stirring for 5 days at r.t., the solvent was removed under reduced pressure, and the crude product purified by flash chromatography (using, in the sequence, $CHCl_3$, $CHCl_3$/EtOH 200:1, 100:1, 70:1, 40:1, 25:1 as eluent) to afford 4.8 mg of 10+ (yield 19%) as a brown solid. R_f (9:1 $CHCl_3$/EtOH) = 0.6; R_f (8:1 toluene/EtOH) = 0.2. ^{1}H NMR ($CDCl_3$) δ −4.45 (s, *ortho*-H_2), −4.49 (t, J = 41 Hz, HD).

Boc-Ala-(H_2@Fp). To a solution of 30 mg (0.042 mmol, 1 equiv) of a 1:1 mixture of H_2@C_{60}/C_{60} in 50 mL of toluene, 13.8 mg (0.042 mmol, 1 equiv) of 3-trityl-5-oxazolidinone was added and the mixture was refluxed for 16 h. The brown mixture was left to cool down to r. t., was concentrated up to 10 mL and then 0.1 mL of CF_3SO_3H was added to remove the trityl moiety. After stirring for 1 h at r. t., the solvent was evaporated under reduced pressure, and the resulting solid washed with 3 × 25 mL of diethyl ether in a centrifuge tube before adding 25 mL of toluene and 90 μL of DIEA. After flash chromatographic purification (95:5 toluene/ethyl acetate), 10 mg (33% w/w) of unreacted H_2@C_{60}/C_{60} was separated, and the solution containing 3,4-fulleropyrrolidine was immediately reacted with (Boc-Ala)$_2$O at 0°C. After stirring at r. t. for 30 min, the solution was purified by flash chromatography (95:5 toluene/ethyl acetate). The solvent was removed under reduced pressure and crystallization from toluene/acetonitrile afforded 8.1 mg of Boc-Ala-(H_2@Fp/Fp) as a brown solid (yield 21%). R_f (7:1 toluene/ethyl acetate) = 0.45. ^{1}H NMR ($CDCl_3$) δ −4.49 (s, *ortho*-H_2), −4.53 (t, J = 41 Hz, HD), 1.48 (s, 9H, *t*Bu), 1.66 (d, J = 7 Hz, 3H, Ala CH_3), 5.03 (q, J = 7 Hz, 1H, Ala CH), 5.53 (m, 5H, NH + Fp $2CH_2$).

Piv-TOAC-(Aib)$_2$-Ala-(H_2@Fp) (10−). 3 mg (0.0075 mmol, 1 equiv) of Piv-TOAC-(Aib)$_2$-OH and 1.45 mg (0.008 mmol, 1.2 equiv) of EDC•HCl were dissolved in 5 mL of anhydrous $CHCl_3$. After stirring at r.t. for 1 h, the solution was cooled down to 0°C and 2.1 μL (0.018 mmol, 3 equiv) of DIEA and TFA·H-Ala-(H_2@Fp/Fp), freshly prepared by treatment of 7.6 mg (0.00825 mmol, 1.1 equiv) of Boc-Ala-(H_2@Fp/Fp) with TFA in $CHCl_3$, were added. After 7 days of stirring at r.t., the solvent was removed under reduced pressure, and the reaction mixture was purified by flash chromatography using $CHCl_3$ followed by mixtures $CHCl_3$/EtOH (v/v 200/1, 100/1, 50/1) as eluents to yield 0.87 mg of 10− (yield 9%) as a brown solid. R_f (9:1 $CHCl_3$/EtOH) = 0.4; R_f (8:1 toluene/EtOH) = 0.2. ^{1}H NMR ($CDCl_3$) δ −4.49 (s, *ortho*-H_2), −4.53 (t, J = 41 Hz, HD).

Methods

Flash chromatography was carried out with silica gel 60 M (0.04–0.063 mm, Macherey-Nagel) as stationary phase. For thin layer chromatography (TLC) Macherey-Nagel TLC-cards (0.2 mm silica gel supported on plastic sheets) were used, and the spots were visualized at 254 nm and then after exposure to iodine vapor and $KMnO_4$ aqueous solution. Fulleropyrrolidine derivatives are brown and thus visible in TLC without staining. The reaction products were dissolved in a minimum amount of solvent and purified by column chromatography. ^{1}H NMR spectra were obtained with a Bruker model Ascend 500 spectrometer, operating at 500 MHz. Deuteriochloroform ($CDCl_3$; 99.8%, *d*; Aldrich) was used as the solvent. Chemical shifts (δ) are given as parts per million (ppm) downfield from tetramethylsilane (TMS).

DFT calculations. The structures of 8+ and 8− and of the reference peptides 9+ and 9− were constructed with the molecular builder GaussView (27) by fusing C_{60} with the Aib (and TOAC) peptide, in the 3_{10}-helix conformation, via two C–C bonds. Structures were then optimized using density functional theory with the molecular package Gaussian 09 (28), fully relaxing the entire system. The specific level of theory was B3LYP/6–31g(d). Solvent effects were incorporated via a polarizable continuum model (PCM), with $CHCl_3$ as the implicit solvent. @C_{60}/nitroxide distances were extracted from optimized structures, from the midpoint of the nitroxide bond to the center of mass of the C_{60} cage. All optimized structures maintained the 3_{10}-helix conformation (*i.e.* no restrains were necessary). The ^{1}H NMR chemical shifts of the four amide protons were calculated for 9+ and 9− at the same DFT level of theory (at the optimized geometry) using the Gauge-Independent Atomic Orbital (GIAO) method. TMS was used as the reference for the computation of chemical shifts.

Nuclear spin relaxation rate of H_2. Nuclear spin relaxation times for compounds 10+ and 10− were measured in $CDCl_3$, at room temperature, using the standard inversion-recovery technique. The concentration of the samples was ~1 mM. The relaxation rate caused by the paramagnetic species, $1/T_{1,p}$, was calculated based on the equation $1/T_{1,p} = (1/T_{1,obs} - 1/T_{1,d})$, where $T_{1,obs}$ is the observed relaxation time and $T_{1,d}$ is the relaxation time in the absence of the paramagnetic center. For the latter we used 140 ms, the average value previously obtained for the hydroxylamine derivatives (the reduction product of the nitroxide moiety) corresponding to compounds 1–6 in 1,2-dichlorobenzene-d_4 (10). It was found previously (29) that $T_{1,d}$ for *endo*-H_2 in H_2@C_{60} is insensitive to solvent because it is isolated from the external medium. We are therefore confident that the $T_{1,d}$ value in 1,2-dichlorobenzene-d_4 should closely approximate that in $CDCl_3$.

Ortho/para H_2 conversion. For both 10+ and 10−, the *ortho*-H_2 to *para*-H_2 conversion was carried out according to the published procedure (13,30) on samples containing *endo*-HD as a standard. A quantity of 1 mg of either 10+ or 10− was dissolved in 1 mL of $CHCl_3$ and then diluted with 35 ml of hexane. NaY zeolite was added to the solution and stirred for 2 h at room temperature, after which the solvent was evaporated under vacuum. The so-obtained mixture of supramolecular complexes was immersed in liquid oxygen at 77 K for 30 min and then the oxygen was rapidly removed under vacuum while still at 77 K. Then, the solid mixture was warmed up to room temperature, to remove liquid nitrogen. The compound was extracted from the zeolite complex with $CHCl_3$, and the solid zeolite was discarded by centrifugation. Chloroform was then removed under vacuum leaving a solid sample of 10+ or 10−. The solid was redissolved in $CDCl_3$, the solution was purged with argon and the sealed sample was analyzed by ^{1}H NMR spectroscopy. Right after the initial conversion, the *ortho*-H_2/*para*-H_2 ratio is reduced from an initial 75% to a 50%. On the other hand, the HD triplet intensity does not change over time, and acts as an internal standard (2). Due to the presence of nitroxide acting as the spin catalyst, the *para*-H_2 is slowly converted back to *ortho*-H_2 and an increment of the ^{1}H NMR signal pertaining to *ortho*-H_2 is thus observable over time. At the end of the conversion process, the ^{1}H NMR signal intensity of *ortho*-H_2 is undistinguishable from that observed before the *ortho–para* conversion.

RESULTS AND DISCUSSION

DFT results

Validation of the *ad hoc* molecular models, obtained as described in Materials and Methods, was first carried out by comparing the ^{1}H NMR chemical shifts of the amide protons for 9+ and 9− with available experimental results of these same systems (25). Figure 1 shows the computed and experimental ^{1}H NMR chemical shifts, and the corresponding structures in the insets. Despite a slight overall shift, the comparison between DFT calculations and experiments is remarkable. As a general observation, relative downfield values are associated with NH groups participating in hydrogen bonds (a more unshielded proton) while upfield values imply a proton not involved in hydrogen bonds (more shielded). Such behavior is consistent with previous experimental and theoretical studies of gold nanoclusters protected by the same type of oligopeptides (31,32). Therefore, besides validating the molecular models, these results confirm that the substantial downfield in the H1 resonance for 9+ (also observed with 8+ (25) and, consequently, also valid for 10+) is due to a strong interaction between H1 and both the N-terminus and the nearest C neighbors from the fullerene (*i.e.* strong unshielding of H1), which points to more robustness of the "+" systems compared to the

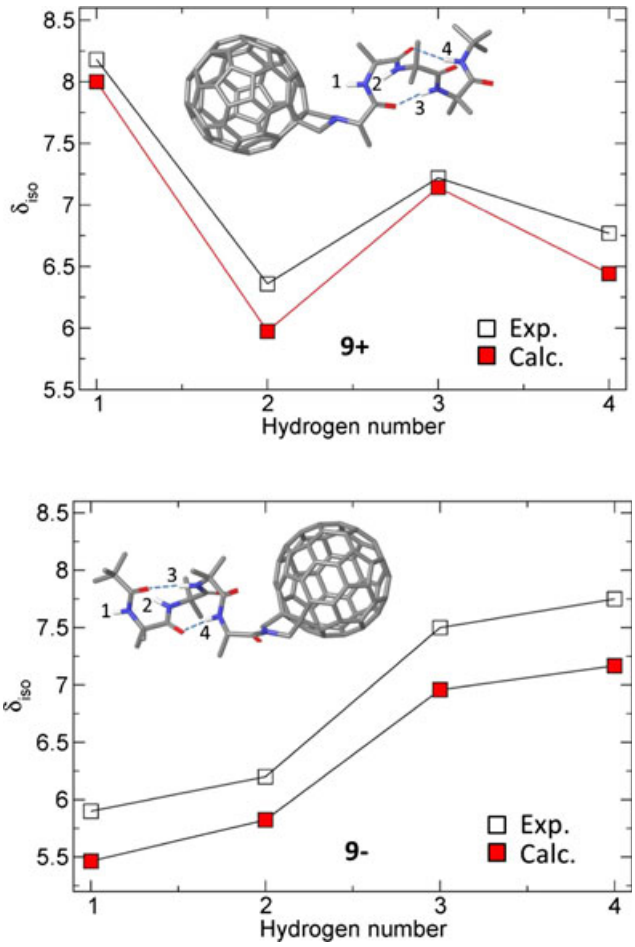

Figure 1. Comparison between experimental (open squares) (25) and calculated (red squares) chemical shifts for the four amide N–H resonances of the investigated peptides ("+" series, top graph; "−" series, bottom graph) in $CDCl_3$. The numbers near the structures label the various N–H groups (numbered from the N- to the C-terminus).

"−" systems, in which such interaction cannot exist. Having confidence in the molecular models of 9+ and 9−, we can now analyze structural features in the TOAC-containing molecular analogues 8+ and 8−. As in the case of 9+ and 9−, the 3_{10}-helix conformation remained intact after optimization. According to these models, the distance r between the center of mass of the fullerene and the midpoint of the nitroxide bond for 8+ and 8− is 14.6 Å and 15.2 Å, respectively, which virtually reflects the fact that the peptide bridge of the "−" series is longer than that of the "+" series by one C–C bond. This estimate of r should closely approximate the average distance between the nitroxide and the center of the *endo*-H_2 molecule. Figure 2 shows the optimized structures. We will use the same distances also for 10+ and 10−.

Nuclear spin relaxation rates

The ^{1}H NMR spectra of the endofullerene–peptide–nitroxide systems 10+ and 10−, obtained in $CDCl_3$, exhibit chemical shifts of the *endo*-H_2 resonance at −4.45 and −4.49 ppm, respectively (Fig. 3). To measure the nuclear spin relaxation times T_1, we used the standard inversion-recovery method, where the nuclear spin polarization is inverted by a π pulse and the corresponding

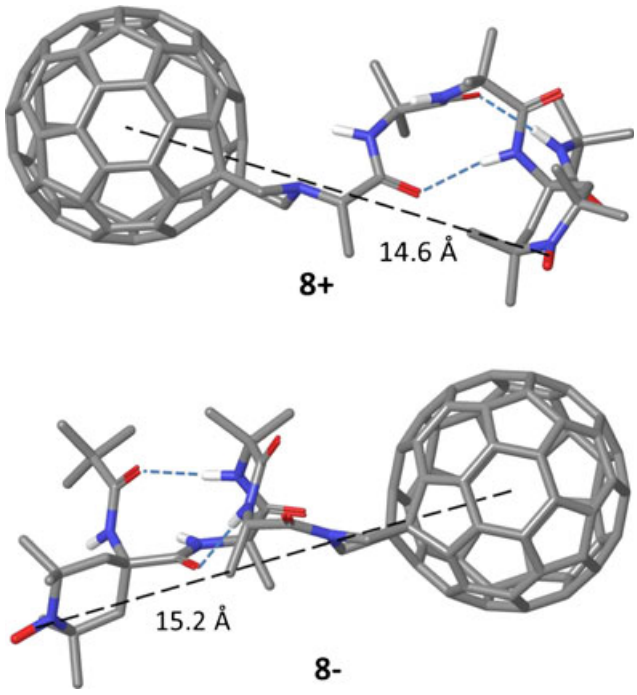

Figure 2. DFT-optimized structures of 8+ (top) and 8− (bottom). Distances are measured from the center of the NO bond to the center of mass of C_{60}.

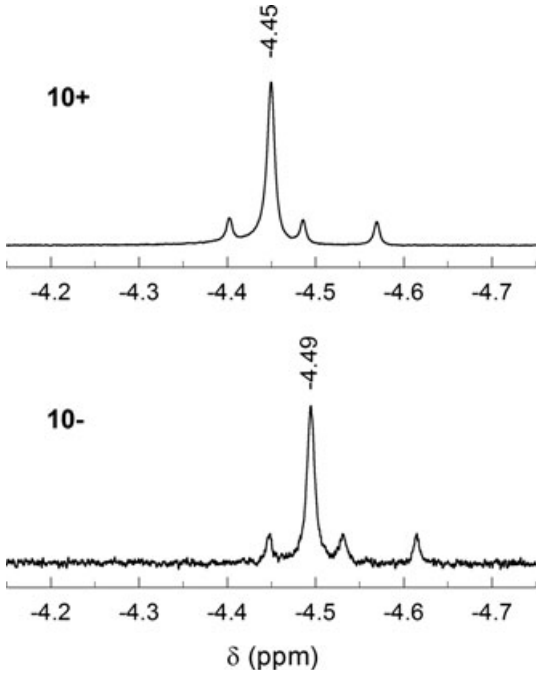

Figure 3. ^{1}H NMR spectra of the *endo*-H_2 region of 10+ (top) and 10− (bottom) in $CDCl_3$. The peaks at −4.45 and −4.49 ppm are the *endo*-H_2 resonances, whereas the surrounding triplets are from HD.

free-induction decay is detected at different delay times by applying a π/2 pulse. An exponential equation is then used to fit the resulting signal intensity to yield the corresponding observed T_1 values (Table 1), which fall in the expected distance range (10). We note that $T_{1,obs}$ for the incarcerated hydrogen in the

Table 1. Relaxation rates, conversion lifetimes and rate constants of 10+ and 10−.

	Distance*(Å)	$T_{1,obs}$ (ms)	$1/T_{1,p}$†(s^{-1})	t_{obs}‡(h)	$10^6 \times (k_{p\text{-}o})_{obs}$§($s^{-1}$)
10+	14.6	108 ± 5	2.1 ± 0.6	125 ± 20	2.22 ± 0.36
10−	15.2	79 ± 4	5.5 ± 0.7	78 ± 5	3.56 ± 0.23

*Distance from the center of the NO bond to the center of C_{60} (from the DFT calculations). †$1/T_{1,p} = (1/T_{1,obs} - 1/T_{1,d})$, where $T_{1,d}$ = 140 ms (10). ‡*para*-H_2 → *ortho*-H_2 conversion lifetime. §Observed $k_{p\text{-}o}$ values.

10− sample is significantly smaller, *i.e.* relaxation is faster than that for 10+.

According to our previous observation in 1,2-dichlorobenzene-d_4 (10), by correcting the observed relaxation time for the average value of the corresponding diamagnetic species ($T_{1,d}$ = 140 ms), the relaxation rates caused by the paramagnetic species, $1/T_{1,p}$, are inversely proportional to the sixth power of the distance r, as predicted by the Solomon–Bloembergen equation (11,12). $1/T_{1,p}$ was originally plotted against the distance obtained for compounds 1–6 (cf Scheme 1) from molecular models, but without applying an energy minimization protocol and rotamers considerations. The apparent distances spanned the range from 0.7 to 1.6 nm. Because of the unique features of Aib peptides, which are rigid even when short, we speculated that 10+ and 10− could furnish sort of reference compounds on the long-distance side of the range. Thus, we will use the values of r obtained from DFT as good approximations of the "true" values.

Before introducing a comparison of previous results (10) with those obtained with 10+ and 10−, it is important to make some introductory remarks. In an earlier report (33) of relaxation in nitroxides 1 and 2, the contribution of the Fermi contact mechanism was found to be negligible. Very recent calculations also showed that both the Fermi contact and Curie interactions are negligible, *i.e.* that relaxation is dominated by the dipolar mechanism (34). Finally, we have already shown that at the concentration here utilized (1 mM) the intermolecular contribution to T_1 is insignificant (10). $1/T_{1,p}$ is thus given by eq. 1, which only refers to the dipolar contribution to the relaxation rate (11,12):

$$\frac{1}{T_{1,p}} = \frac{2}{15}\left(\frac{\mu_0}{4\pi}\right)^2 \left[\frac{\gamma_I^2 g^2 \mu_B^2 S(S+1)}{r^6}\right]\left[\frac{3\tau_c}{1+\omega_I^2\tau_c^2} + \frac{7\tau_c}{1+\omega_S^2\tau_c^2}\right] = \frac{A}{r^6} \quad (1)$$

where γ_I is magnetogyric ratio of the nucleus that is being relaxed (H), g is the electronic g factor, μ_B is the Bohr magneton, r is the distance between the proton and the unpaired electron in the complex, S is the spin quantum number (1/2 for nitroxide), ω_I and ω_S are the nuclear and electronic Larmor frequencies, respectively, and τ_c is the global correlation time. τ_c essentially corresponds to the rotational correlation time of the molecule, τ_r (34).

We previously assumed that τ_c is only slightly affected by the C_{60} functionalization (10), an assumption that is supported by DFT calculations (34). Here, as explained below, we consider that the impact of the peptide-TOAC moiety on τ_c is also negligible. For values of τ_c longer than the reciprocal of the electron Larmor frequency ($1/\omega_S = 5 \times 10^{-13}$ s, for 500 MHz ^{1}H NMR), the second term in the last parenthesis of Eq. (1) is negligible. As values of τ_c for the fullerene nitroxides are longer than 10^{-11} s (10,34), $1/T_{1,p}$ should therefore be approximately proportional to τ_c. We have already specified the difference between the solvent employed in reference 10 and in this study (for solubility reasons). The correlation time τ_c of Eq. (1) is related to the solvent viscosity η through the Stokes–Debye–Einstein equation $\tau_c = (4\pi/3)a^3\eta/k_BT$, where a is the average effective radius of the molecule. Thus, τ_c is expected to decrease by a factor 0.41 and, therefore, the value of $1/T_{1,p}$ should decrease as one goes from chloroform to 1,2-dichlorobenzene (η = 0.54 and 1.32 cP, respectively, at 25°C [35]), provided that the value of a does not change. On one hand, because of the dependence of $1/T_{1,p}$ on r^{-6}, this difference has a very small effect when considering long distances. On the other hand, τ_c also depends on a^3 and peptides 10+ and 10− are larger than molecules 1–6, and this parameter tends to compensate the lower viscosity of chloroform: for example, an increase of 2 Å in the average molecular radius would make the product $a^3\eta$ virtually unchanged. On these grounds, we believe that the $1/T_{1,p}$ values of 10+ and 10− can be directly compared to those of 1–6. Similarly, this justifies the use of the previously determined $1/T_{1,d}$ average value for correcting the experimental $T_{1,obs}$ values.

For 10+ and 10−, the $1/T_{1,p}$ values of Table 1 were thus calculated from $1/T_{1,obs}$ by subtracting the contribution of the diamagnetic reference ($1/T_{1,d}$, where $T_{1,d}$ = 140 ms) and considering the overall uncertainty associated with the T_1 values (ca. 5%, i.e., as found for 1–6 [10]). Figure 4 was obtained using the DFT distances pertaining to 10+ and 10−, and applying the same analysis previously used for compounds 1–6, in which the distances were estimated by molecular modeling. Figure 4

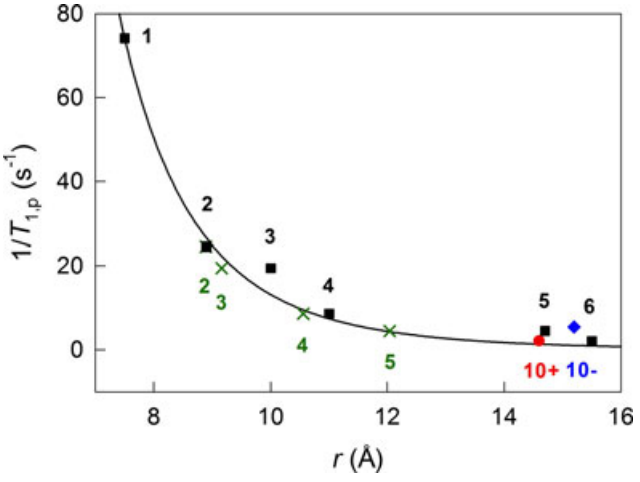

Figure 4. $1/T_{1,p}$ *vs* calculated distances for 10+ (●), 10− (◆) and 1–6 (■: from reference 10) The curve fitting the results obtained with 1–6 and 10+ is based on Eq. (1) (see text). The uncertainty associated with the $1/T_{1,p}$ values was estimated by assuming an error of 5% in the values of $1/T_{1,obs}$ and $1/T_{1,d}$, as in previous work (10,29). Some of the $1/T_{1,p}$ data are also plotted against more recent r estimates (34) for 2–5 (×).

shows that in spite of the very similar distances, whereas the relaxation rate of 10+ follows the overall trend very nicely, the relaxation rate of 10− rests detectably above the plot. The curve of $1/T_{1,p}$ *vs* r^{-6} was calculated by using the values of $1/T_{1,p}$ and r for compound 1, taken as the most stereochemically rigid, to determine the proportionality constant A of Eq. (1). The fact that 10− provides a value of $1/T_{1,p}$ larger than expected may be related to a significantly smaller effective distance. That this could be indeed the case is nicely supported by recent DFT determinations of the distances of compounds 2–5 (34), which led to r values much closer to the fitting curve, as shown in Fig. 4. In particular, the r values of compounds 3 and 5, which appear as particularly off from the trend line, were found to be smaller by 0.84 and 2.66 Å, respectively. On this basis, we use the $1/T_{1,p}$ *vs* r plot to estimate for 10− an effective distance r of 11.6 Å. Overall, these new results thus confirm that the overall trend observed previously (10) was sufficiently accurate despite the spacers connecting the nitroxide radical and the C_{60} cage were relatively flexible compared with the peptide bridges of 10+ and 10−.

The rigidity of the helical backbones of 10+ and 10−, however, stimulates further considerations. Let us start by noticing that the fullerene and the radical moieties of 10+ and 10− are connected by a quite similar number of bonds (from C_{60} to the nitroxide nitrogen, 15 and 16 bonds, respectively). However, in our previous study of fullerene–Aib–peptide–nitroxide systems (25), we showed how the possible rotamers of the "+" series are drastically reduced due to presence of the hydrogen bond involving the first amide proton, an interaction that here we have confirmed by DFT calculations (cf Fig. 1). As detailed in the Introduction, time-resolved EPR results showed that the spin exchange coupling between the singlet state of the free radical and the triplet state of the photoexcited fullerene is stronger in 8− than in 8+ due to different orientations of the pairs in the two cases and thus to the different way by which the helix is oriented. That the results pointed to a less stiff system for 8−, which provides more opportunities of optimizing the radical–triplet pair coupling, was in keeping with the IR and NMR results that concurred to indicate that the 8+ is stiffer. All these conclusions can be applied also to systems 10+ and 10−. If we now consider the nuclear spin relaxation rates of 10+ and 10−, Fig. 4 also suggests that system 10− (but not the helical backbone itself, which in 10− is as rigid as in 10+) is more flexible than 10+, in the sense that on the investigated time scale, the nitroxide could happen to be closer by 3.6 Å to $H_2@C_{60}$ than the optimized structure of Fig. 2 would indicate. Concerning 10+, however, the overall structure is such to keep $H_2@C_{60}$ and nitroxide as rigidly separated as possible: this allows for only a weak interaction between the nitroxide and the incarcerated H_2 and, therefore, results in a longer nuclear longitudinal relaxation time. In this sense, we can take the $1/T_{1,p}$ value of 10+ as a particularly solid data point of the correlation of Fig. 4.

Para-H_2 to *ortho*-H_2 conversion

The observation of a significant difference between the nuclear spin relaxation rates of the two endohedral-fullerene peptides prompted us to obtain also the corresponding *para* → *ortho* conversion rates. As described in the Introduction, at 77 K the NMR active *ortho*-H_2 of endohedral fullerenes can be made to exist in an equimolar ratio with the NMR inactive *para*-H_2. By taking the samples to room temperature, *para*-H_2 converts to *ortho*-H_2 to reach the room-temperature *para*-H_2 to *ortho*-H_2 equilibrium ratio of 25%: 75%. This conversion is studied by monitoring the increase in intensity of the *ortho*-H_2 resonance. The conversion process is catalyzed by the nitroxide radical linked through the molecular bridge to the $H_2@C_{60}$ moiety, and the rate thus depends on their relative distance (13). We carried out the same experiments on 10+ and 10−. Figure 5 compares the transients corresponding to the slow increase of the ^{1}H NMR signal of the *ortho*-H_2 resonance of the two peptides. From the exponential increase, for the conversion lifetimes of 10+ and 10− we calculated 125 and 78 h, respectively (Table 1). The corresponding rate constants $k_{p\text{-}o}$ were calculated by subtracting from the observed rate constant the rate constant of the reference compound 7 (which contains no radical catalyst) and multiplying by ¾ to take into account the contribution from the reverse rate, as already discussed (13). Despite the very similar DFT r values,

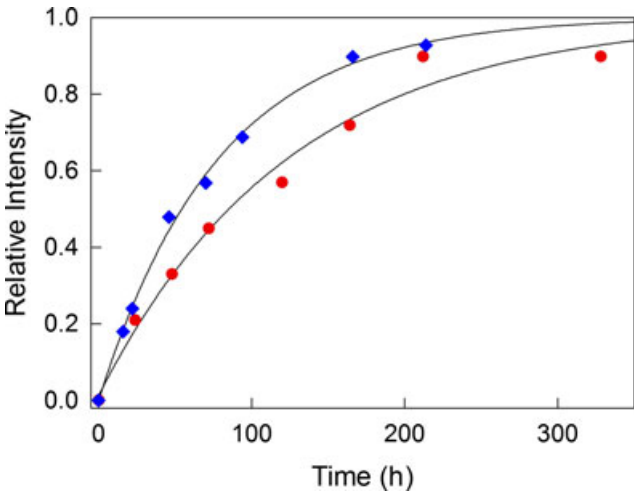

Figure 5. *Para*-H_2 to *ortho*-H_2 conversion time profile for 10+ (●) and 10− (◆).

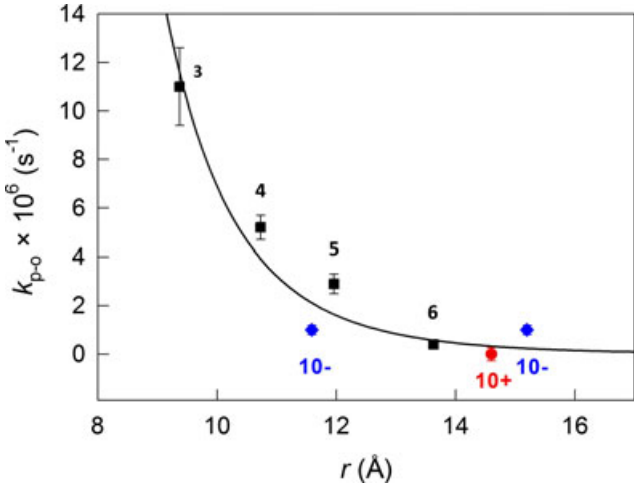

Figure 6. Dependence of the *para*-H_2 → *ortho*-H_2 conversion rate constant $k_{p\text{-}o}$, corrected for the diamagnetic reference, on the $H_2@C_{60}$/nitroxide distance r. The results pertain to 10+ (●), 10− (◆) and 3–6 (■: from reference 13). The curve shows the $k_{p\text{-}o}$ *vs* $1/r^8$ best fit to the results obtained for 3–6 and 10+ . For 10−, $k_{p\text{-}o}$ is given as a function of both the $T_{1,p}$ estimated (left-hand side) and DFT (right-hand side) r values.

the large difference between the conversion rates of 10+ and 10− is worth noting.

As already suggested, the intramolecular version of Wigner's theory, which predicts that the *para*-H_2 → *ortho*-H_2 conversion rate of the endohedral H_2 should vary with r^{-8}, is satisfactorily obeyed by compounds 3–6 (the conversions of 1 and 2 were too fast to be monitored within the time required for working up the samples) (13). Figure 6 shows the plot of $k_{p\text{-}o}$ *vs r*, in which the results obtained for compounds 10+ and 10− are compared with those obtained for 3–6. On the basis of the excellent fit of the $1/T_{1,p}$ *vs* r^{-6} equation to the experimental data, to make Fig. 6 we used the effective distances induced from the relaxivity plot. This was done for all compounds except for 10+ whose DFT *r* value is considered to be particularly accurate; the $k_{p\text{-}o}$ of 10− is also shown as a function of its DFT *r* value.

It is found that the values of $k_{p\text{-}o}$ fall monotonically with the $1/T_{1,p}$ estimates of the distance. The *para*-H_2 to *ortho*-H_2 conversion results are thus consistent with the relative relaxivity rates of 10+, 10− and nitroxides 1–6. The general trend of the results shown in Fig. 6 is in satisfactory agreement with the Wigner's theory modified for the intramolecular interaction of H_2 with the nitroxide (13–15), in which $k_{p\text{-}o}$ is expected to depend on $1/r^8$, as evidenced by the corresponding interpolation curve, obtained for the data pertaining to 3–6 and 10+. Figure 6 also shows that on the basis of the correlation, the effective *r* distance of 10− appears to be in between the $1/T_{1,p}$ estimate and the DFT value, although still significantly smaller than the latter. The observed value of $k_{p\text{-}o}$ for 10+, on the other hand, shows that for this compound the nitroxide radical has, within experimental error, virtually no effect on the *para*-H_2 to *ortho*-H_2 conversion rate of the nitroxide and endohedral H_2. This further confirms that the 10+ system is rigid and with the two interacting moieties particularly well separated.

Acknowledgements—This work was financially supported by the Italian Ministry of Education, University and Research (PRIN 20098Z4M5E), the University of Padova (PRAT CPDA103389) and the National Science Foundation (grant CHE 11-11392).

REFERENCES

1. Komatsu, K., M. Murata and Y. Murata (2005) Encapsulation of molecular hydrogen in fullerene C_{60} by organic synthesis. *Science* **307**, 238–240.
2. Turro, N. J., J. Y.-C. Chen, E. Sartori, M. Ruzzi, A. Martí, R. G. Lawler, S. Jockusch, J. Lopez-Gejo, K. Komatsu and Y. Murata (2010) The spin chemistry and magnetic resonance of $H_2@C_{60}$. From the Pauli principle to trapping a long lived nuclear excited spin state inside a buckyball. *Acc. Chem. Res.* **43**, 335–345.
3. Rodriguez-Fortea, A., A. L. Balch and J. M. Poblet (2011) Endohedral metallofullerenes: a unique host-guest association. *Chem. Soc. Rev.* **40**, 3551–3563.
4. López-Gejo, J., A. A. Martí, M. Ruzzi, S. Jockusch, K. Komatsu, F. Tanabe, Y. Murata and N. J. Turro (2007) Can H_2 Inside C_{60} Communicate with the Outside World? *J. Am. Chem. Soc.* **129**, 14554–14555.
5. Frunzi, M., S. Jockusch, J. Y.-C. Chen, R. M. Krick Calderon, X. Lei, Y. Murata, K. Komatsu, D. M. Guldi, R. G. Lawler and N. J. Turro (2011) A photochemical on-off switch for tuning the equilibrium mixture of H_2 nuclear spin isomers as a function of temperature. *J. Am. Chem. Soc.* **133**, 14232–14235.
6. Chen, J. Y.-C., Y. Li, M. Frunzi, X. Lei, Y. Murata, R. G. Lawler and N. J. Turro (2013) Nuclear spin isomers of guest molecules in $H_2@C_{60}$, $H_2O@C_{60}$ and other endofullerenes. *Phil. Trans. R. Soc. A* **371**, 20110628.
7. Schubert, C., M. Rudolf, D. M. Guldi, Y. Takano, N. Mizorogi, M. Ángeles Herranz, N. Martin, S. Nagasi and T. Akasaka (2013) Rates and energetics of intramolecular electron transfer processes in conjugated metallofullerenes. *Phil. Trans. R. Soc. A* **371**, 20120490.
8. Filidou, V., S. Mamone, S. Simmons, S. D. Karlen, H. L. Anderson, C. W. M. Kay, A. Bagno, F. Rastrelli, Y. Murata, K. Komatsu, X. Lei, Y. Li, N. J. Turro, M. H. Levitt and J. J. L. Morton (2013) Probing the C_{60} triplet state coupling to nuclear spins inside and out. *Phil. Trans. R. Soc. A* **371**, 20120475.
9. Zoleo, A., R. G. Lawler, X. Lei, Y. Li, Y. Murata, K. Komatsu, M. Di Valentin, M. Ruzzi and N. J. Turro (2012) ENDOR evidence of electron-H_2 interaction in a fulleride embedding H_2. *J. Am. Chem. Soc.* **134**, 12881–12884.
10. Li, Y., X. Lei, R. G. Lawler, Y. Murata, K. Komatsu and N. J. Turro (2010) Distance-dependent paramagnet enhanced nuclear spin relaxation of $H_2@C_{60}$ derivatives covalently linked to a nitroxide radical. *J. Phys. Chem. Lett.* **1**, 2135–2138.
11. Solomon, I. (1955) Relaxation processes in a system of two spins. *Phys. Rev.* **99**, 559–565
12. Bloembergen, N. and L. O. Morgan (1961) Proton relaxation times in paramagnetic solutions. Effects of electron spin relaxation. *J. Phys. Chem.* **34**, 842–850.
13. Li, Y., X. Lei, R. G. Lawler, Y. Murata, K. Komatsu and N. J. Turro (2011) Distance-dependent *para*-H_2→*ortho*-H_2 conversion in $H_2@C_{60}$ derivatives covalently linked to a nitroxide radical. *J. Phys. Chem. Lett.* **2**, 741–744.
14. Wigner, E. Z. (1933) Concerning the paramagnetic conversion of *para-ortho* Hydrogen. III. *Phys. Chem.* **B23**, 28–32
15. Atkins, P. W. and M. J. Clugston (1974) *ortho-para* Hydrogen conversion in paramagnetic solutions. *Mol. Phys.* **27**, 1619–1631.
16. Toniolo, C., G. M. Bonora, V. Barone, A. Bavoso, E. Benedetti, B. Di Blasio, P. Grimaldi, F. Lelj, V. Pavone and C. Pedone (1985) Conformation of pleionomers of α-aminoisobutyric acid. *Macromolecules* **18**, 895–902
17. Toniolo, C. and E. Benedetti (1991) The polypeptide 3_{10}-helix. *Trends Biochem. Sci.* **16**, 350–353.
18. Toniolo, C., M. Crisma, F. Formaggio, C. Peggion, Q. B. Broxterman and B. Kaptein (2004) Molecular spacers for physicochemical investigations based on novel helical and extended peptide structures. *Biopolymers (Pept. Sci.)* **76**, 162–176.
19. Shin, Y.-G., M. D. Newton and S. S. Isied (2003) Distance dependence of electron transfer across peptides with different secondary structures: the role of peptide energetics and electronic coupling. *J. Am. Chem. Soc.* **125**, 3722–3732.
20. Holm, A. H., M. Ceccato, R. L. Donkers, L. Fabris, G. Pace and F. Maran (2006) Effect of peptide ligand dipole moments on the redox potentials of Au_{38} and Au_{140} nanoparticles. *Langmuir* **22**, 10584–10589.
21. Galoppini, E. and M. A. Fox (1996) Effect of the electric field generated by the helix dipole on photoinduced intramolecular electron transfer in dichromophoric α–helical peptides. *J. Am. Chem. Soc.* **118**, 2299–2300.
22. Fox, M. A. and E. Galoppini (1997) Electric fields effect on electron transfer rates in dichromophoric peptides: the effect of helix unfolding. *J. Am. Chem. Soc.* **119**, 5277–5285.
23. Antonello, S., F. Formaggio, A. Moretto, C. Toniolo and F. Maran (2003) Anomalous distance dependence of electron transfer across peptide bridges. *J. Am. Chem. Soc.* **125**, 2874–2875.
24. Polo, F., S. Antonello, F. Formaggio, C. Toniolo and F. Maran (2005) Evidence against the hopping mechanism as an important electron transfer pathway for conformationally constrained oligopeptides. *J. Am. Chem. Soc.* **127**, 492–493.
25. Garbuio, L., S. Antonello, I. Guryanov, Y. Li, M. Ruzzi, N. J. Turro and F. Maran (2012) Effect of orientation of the peptide-bridge dipole moment on the properties of fullerene-peptide-radical systems. *J. Am. Chem. Soc.* **134**, 10628–10637.
26. Toniolo, C., M. Crisma, F. Formaggio and C. Peggion (2001) Control of peptide conformation by the Thorpe Ingold effect (C-alpha tetrasubstitution). *Biopolymers* **60**, 396–419.
27. GaussView, Version 5, Dennington, R., T. Keith and J. Millam, Semichem Inc., Shawnee Mission KS, 2009.
28. Gaussian 09, Revision A.1, Frisch, M. J., G. W. Trucks, H. B. Schlegel, G. E. Scuseria, M. A. Robb, J. R. Cheeseman, G. Scalmani, V. Barone, B. Mennucci, G. A. Petersson, H. Nakatsuji, M.

Caricato, X. Li, H. P. Hratchian, A. F. Izmaylov, J. Bloino, G. Zheng, J. L. Sonnenberg, M. Hada, M. Ehara, K. Toyota, R. Fukuda, J. Hasegawa, M. Ishida, T. Nakajima, Y. Honda, O. Kitao, H. Nakai, T. Vreven, J. A. Montgomery Jr, J. E. Peralta, F. Ogliaro, M. Bearpark, J. J. Heyd, E. Brothers, K. N. Kudin, V. N. Staroverov, R. Kobayashi, J. Normand, K. Raghavachari, A. Rendell, J. C. Burant, S. S. Iyengar, J. Tomasi, M. Cossi, N. Rega, J. M. Millam, M. Klene, J. E. Knox, J. B. Cross, V. Bakken, C. Adamo, J. Jaramillo, R. Gomperts, R. E. Stratmann, O. Yazyev, A. J. Austin, R. Cammi, C. Pomelli, J. W. Ochterski, R. L. Martin, K. Morokuma, V. G. Zakrzewski, G. A. Voth, P. Salvador, J. J. Dannenberg, S. Dapprich, A. D. Daniels, Ö. Farkas, J. B. Foresman, J. V. Ortiz, J. Cioslowski and D. J. Fox, Gaussian, Inc., Wallingford CT, 2009.

29. Sartori, E., M. Ruzzi, N. J. Turro, J. D. Decatur, D. C. Doetschman, R. G. Lawler, A. L. Buchachenko, Y. Murata and K. Komatsu (2006) Nuclear relaxation of H_2 and $H_2@C_{60}$ in organic solvents. *J. Am. Chem. Soc.* **128**, 14752–14753.
30. Turro, N. J., A. A. Martí, J. Y.-C. Chen, S. Jockusch, R. G. Lawler, M. Ruzzi, E. Sartori, E. S.-C. Chuang, K. Komatsu and Y. Murata (2008) Demonstrations of a chemical transformation inside a fullerene. The reversible conversion of the allotropes of $H_2@C_{60}$. *J. Am. Chem. Soc.* **130**, 10506–10507.
31. Fabris, L., S. Antonello, L. Armelao, R. L. Donkers, F. Polo, C. Toniolo and F. Maran (2006) Gold nanoclusters protected by conformationally constrained peptides. *J. Am. Chem. Soc.* **128**, 326–336.
32. Perera, N. V., W. Isley, W. F. Maran and J. A. Gascón (2010) Molecular modeling characterization of a conformationally constrained monolayer-protected gold cluster. *J. Phys. Chem. C* **114**, 16043–16050.
33. Li, Y., X. Lei, R. G. Lawler, Y. Murata, K. Komatsu and N. J. Turro (2011) Indirect ^{1}H NMR characterization of $H_2@C_{60}$ nitroxide derivatives and their nuclear spin relaxation. *Chem. Commun.* **47**, 12527–12529.
34. Rastrelli, F., D. Frezzato, R. G. Lawler, Y. Li, N. J. Turro and A. Bagno (2013) Predicting the paramagnet-enhanced NMR relaxation of H_2 encapsulated in endofullerene nitroxides by density-functional theory calculations. *Phil. Trans. R. Soc. A* **371**, 20110634.
35. CRC Handbook of Chemistry and Physics, 85th Edition, David. R. Lide, ed., CRC Press, Boca Raton, FL, 2004.